FOR THE RECORD

Toward the functional oligomerization state of tryptophan-rich sensory proteins

Łukasz Jaremko,[1,2] Mariusz Jaremko,[1] Stefan Becker,[1] and Markus Zweckstetter[1,2,3]*

[1]Max-Planck-Institut für Biophysikalische Chemie, 37077 Göttingen, Germany
[2]Deutsches Zentrum für Neurodegenerative Erkrankungen (DZNE), 37077 Göttingen, Germany
[3]Center for Nanoscale Microscopy and Molecular Physiology of the Brain, University Medical Center, 37073 Göttingen, Germany

Received 4 April 2014; Accepted 7 May 2014
DOI: 10.1002/pro.2487
Published online 10 May 2014 proteinscience.org

Abstract: A conserved family of tryptophan-rich sensory proteins (TspO) mediates the transport of heme degradation intermediates across membranes. In eukaryotes, the homologous mitochondrial translocator protein (TSPO) binds cholesterol and radioligands as monomer. On the basis of the mammalian TSPO structure, bioinformatic analysis, and a 10 Å resolution electron microscopy map of TspO from *Rhodobacter sphaeroides*, we developed a model of the tertiary and quaternary structure of TspO that is in agreement with available mutagenesis data. Our study provides insight into the conformational basis for the restricted interaction of bacterial TspO with radioligands and the functional oligomerization state of bacterial TspO proteins.

Keywords: mitochondria; membrane protein; receptor; structure; oligomerization

Introduction

Cell membranes of living organisms are formed by lipid bilayers that are largely impermeable to ions and small molecule metabolites. The movement of small compounds through the cell membranes is enabled by transmembrane proteins forming pores, channels and gates. The translocator protein (tryptophan-rich sensory protein, TSPO), present in mitochondria of eukaryotes, is an 18 kDa protein, which is mainly found at the outer and inner membrane contact sites[1,2] and mediates the transport of porphyrins and dicarboxylic tetrapyrrole products of the heme biosynthetic pathway. Additionally, TSPO is known for its interaction with the steroidogenic acute regulatory protein to transport cholesterol into mitochondria.[3,4] At the carboxylic terminus, TSPO contains a high-affinity cholesterol recognition amino-acids consensus sequence.[5] The mitochondrial TSPO was first described as peripheral benzodiazepine receptor (PBR), a secondary binding site for diazepam,[6,7] but subsequently the receptor was found to be expressed throughout the body, including brain.[8] The TSPO was found to interact with VDAC and ANT,[9] which may be part of its capability to regulate the collapse of the mitochondrial membrane potential.[10] Transmission electron and atomic force

Additional Supporting Information may be found in the online version of this article.

Łukasz Jaremko and Mariusz Jaremko contributed equally to this work.

Grant sponsor: Deutsche Forschungsgemeinschaft Collaborative Research Center 803, Project A11. Grant sponsor: European Research Council; Grant number: 282008.

*Correspondence to: Markus Zweckstetter, Deutsches Zentrum für Neurodegenerative Erkrankungen (DZNE) c/o Max-Planck-Institut für Biophysikalische Chemie, Am Fassberg 11, 37077 Göttingen, Germany. E-mail: markus.zweckstetter@dzne.de

microscopy indicated that between four to six molecules of TSPO preferentially associate with one molecule of VDAC to form a single mitochondrial pore.[11]

The TSPO architecture is highly dynamic in the ligand-free state.[12,13] Synthetic ligands such as 1-(2-chlorophenyl)-*N*-methyl-*N*-(1-methylpropyl)−3-isoquinoline-carboxamide (PK 11195) bind to TSPO[14–16] and decrease its flexibility.[12,13] The ligand-induced structural stabilization enabled the determination of the three-dimensional structure of mouse TSPO (*m*TSPO) using solution-state nuclear magnetic resonance (NMR) spectroscopy.[12] The 3D structure of the mTSPO–PK 11195 complex is composed of five transmembrane α-helices (TM1 to TM5) that tightly pack together in the clockwise order TM1–TM2–TM5–TM4–TM3 (cytosolic view). The longest loop is located in between the helices TM1 and TM2 and closes the entrance to the hydrophobic pocket where PK 11195 is bound. The TSPO–PK 11195 complex contains one TSPO and one PK 11195 molecule, in agreement with a 1:1 stoichiometry of TSPO–ligand interactions.[14]

In the case of evolutionary older organisms that lack mitochondria, the prokaryotic tryptophan-rich sensory protein TspO is an ortholog of mammalian TSPO, both proteins belonging to the same TspO/PBR protein family. However, bacterial TspO differs from mitochondrial TSPO in several important aspects such as its affinity to ligands. Although both TspO and TSPO bind the pyrrolidone intermediates of porphyrin degradation,[17] the interaction of the bacterial protein with high-affinity synthetic ligands of mammalian TSPO is perturbed.[18] In addition, the two orthologs differ in their oligomerization state: mammalian TSPO recognizes PK 11195 as a monomer[12] while the bacterial ortholog is dimeric.[19,20] Dimers of TspO from *Rhodobacter sphaeroides* (*Rs*TspO) observed by cryo-electron microscopy (EM) had dimensions of approximately 40 Å × 27 Å × 40 Å. However, due to the limited resolution of the electron density neither the helix topology nor the identity of the helices at the dimer interface was resolved. The distinct oligomerization state of *Rs*TspO and *m*TSPO raises the question about the functional importance of their quaternary structure. Moreover, reactive oxygen species can induce oligomer formation of mammalian TSPO, including dimers, tetramers, and octamers, but the exact functional and pathological role of these oligomers is unknown.[21]

To dissect the dimeric arrangement of *Rs*TspO and the structural basis for the distinct affinity of the bacterial and mammalian protein to synthetic ligands, we here combine the 3D structure of the *m*TSPO–PK 11195 complex with the EM map of *Rs*TspO and homology modeling techniques. The developed 3D model of RsTspO fits and explains the structural and biochemical data presented by others so far. In addition, it highlights differences in ligand binding between mammalian and bacterial orthologs of the protein.

Results

*Rs*TspO shares 32%/55% sequence identity/similarity with *m*TSPO, which itself has a sequence identity of 86% with the human protein (see Supporting Information Fig. S1). Consistent with the high sequence identity, the secondary structure predicted for *Rs*TspO—including the five transmembrane helices—is highly similar to that of mammalian TSPO. Many RsTspO residues that are involved in interhelix contacts in *m*TSPO, such as W5, Y31, L34, P37, W39, V64, W135, and L142[12] are conserved [Fig. 1(A,B)]. In addition, proline 130/138 (*Rs*TspO/*m*TSPO), which induces a kink in the transmembrane helix TM5, is present in both *Rs*TspO and *m*TSPO. The lowest interspecies similarities are found for TM1, with TM1 of *Rs*TspO containing more polar residues when compared to *m*TSPO [Fig. 1(A)].

Next, we determined a 3D homology model of monomeric *Rs*TspO using the Chimera[22] interface to Modeller9v13.[23] The 3D homology model of *Rs*TspO is composed of five transmembrane α-helices [Fig. 1(B)]. Helix TM3 extends slightly less (approximately by one α-helix turn) out of the membrane when compared to *m*TSPO [Fig. 1(B) and Supporting Information Fig. S2]. The five transmembrane helices of *Rs*TspO are connected by short loops. Due to the absence of three amino acids in the bacterial ortholog (^{27}RGE^{29} in *m*TSPO), the extracellular loop connecting TM1 and TM2 is shorter than in *m*TSPO (see Supporting Information Fig. S2). In addition, the TM1–TM2 loop of *Rs*TspO is predicted to be flexible, while this loop forms a well-defined and rigid α-helix (E29 to A35) in the high-resolution 3D structure of the *m*TSPO–PK 11195 complex.[12] This α-helix is part of the lid protecting the entrance to the PK 11195 binding site of *m*TSPO.

The structural model of *Rs*TspO is supported by an analysis of the nuclear Overhauser effect contacts, which were observed in the *m*TSPO–PK 11195 complex between residues that are identical in *m*TSPO and *Rs*TspO [Fig. 1(B)]. In the contact network, TM1 of *Rs*TspO is linked to the neighboring TM3 helix through residue W5 and G22. A further potentially conserved contact is present between Y31 (C-terminal end of TM1) and K36 (N-terminal end of TM2). All other helices are mutually linked in the clockwise order TM2–TM5–TM4–TM3–TM1 (extracellular view). In addition, TM2 has conserved contacts with TM4 and the TM1–TM2 loop is connected to TM5 by the interactions L34–N150 and K36/P37/W39–A100 [Fig. 1(B)]. Overall, a larger number of contacts between conserved residues are present at the side of the *Rs*TspO model, which is distant from the extracellular space. This is due to the higher sequence conservation in this part of the

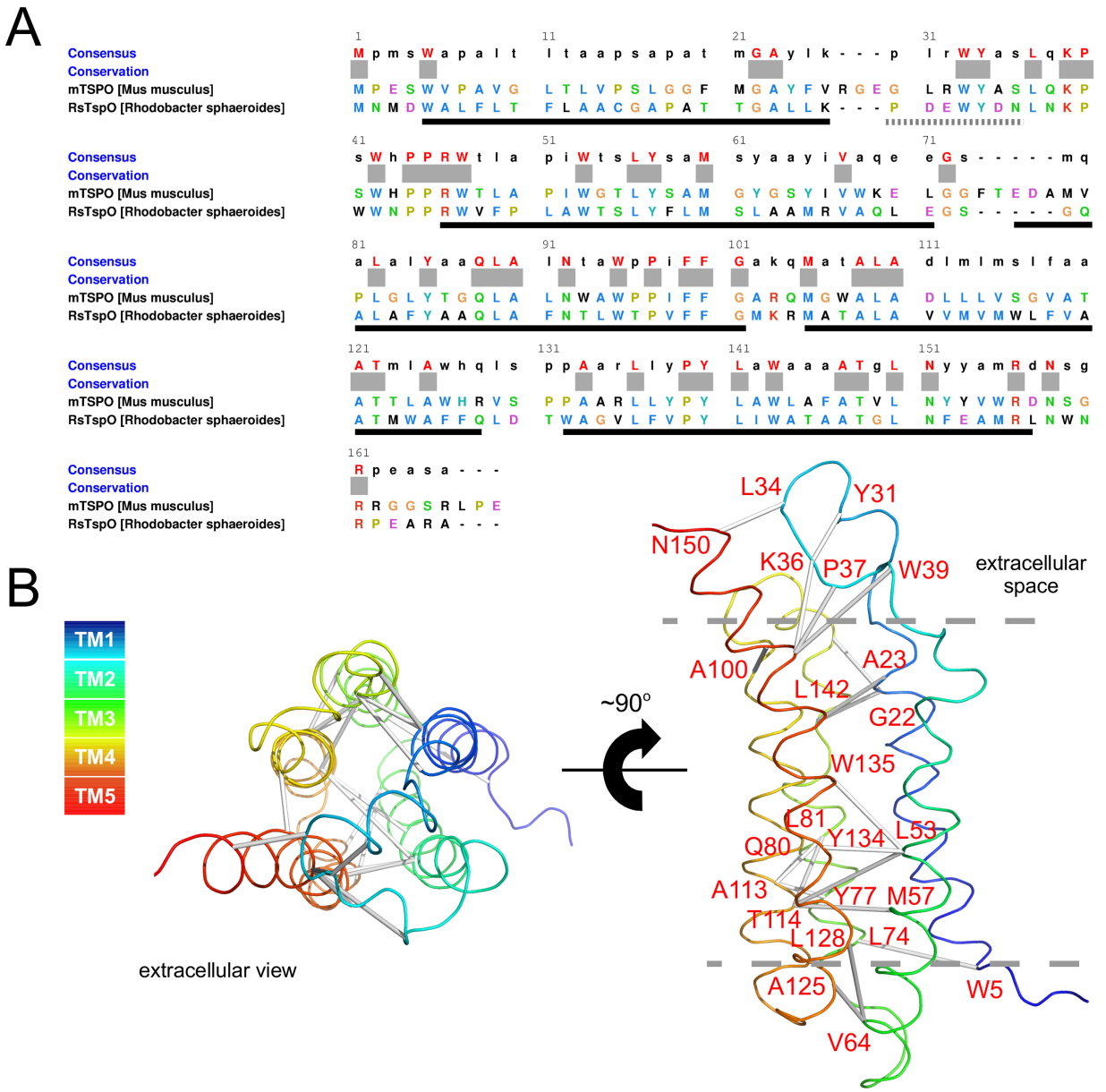

Figure 1. Model of the tertiary structure of *Rs*TspO. A: Sequence alignment of *m*TSPO [Mus Musculus] and *Rs*TspO [*R. sphaeroides*]. Identical residues in the two proteins are marked in red. The location of the five transmembrane helices is indicated by black solid lines. The helix, which is found in the TM1–TM2 loop of the *m*TSPO–PK 11195 complex structure, is marked by a gray dotted line. B: The best-scored 3D homology model of *Rs*TspO with highly conserved residues (red in A) linked by their Cα atoms according to the presence of long-range nuclear Overhauser enhancement cross peaks experimentally observed in the *m*TSPO–PK 11195 complex. Transmembrane helices 1–5 are colored from blue to red. Gray dotted lines indicate approximate membrane boundaries.

protein [Fig. 1(A,B)]. It also suggests that ligand binding to the less conserved extracellular side of *Rs*TspO might be important for structural stabilization. Consistent with this hypothesis the EM map of *Rs*TSPO in the absence of a synthetic ligand was less defined on the extracellular side [Fig. 2(A)].

To obtain structural insight into the oligomerization of *Rs*TspO, we combined the homology model of *Rs*TspO [Fig. 1(B)] with the electron density observed by cryo-EM for *Rs*TspO.[19] Dimeric models of *Rs*TspO were generated using a "pdbsymm" symmetry builder script from the Situs 2.7 package[24] and the modeled 3D structure of *Rs*TspO. The *C*2 axis was defined in front of either the TM1/TM2 helices or the TM2/TM5 helices. The resulting dimer was fitted into the 10 Å EM map using Chimera.[22] The mutual orientation of the subunits was subsequently refined with enforced *C2* symmetry until the maximum correlation between the experimental and simulated dimer maps at 10 Å was achieved.

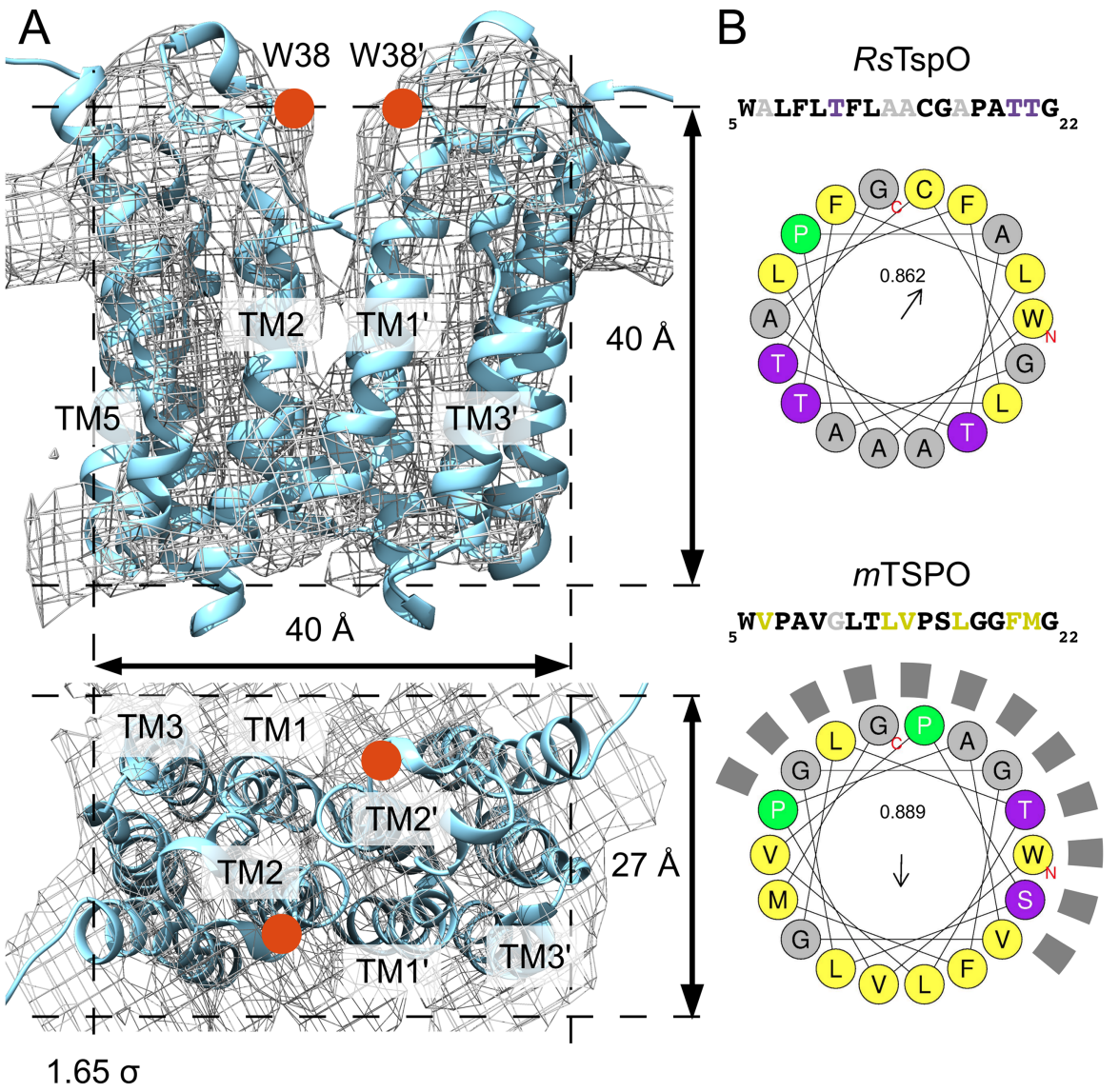

Figure 2. Potential dimeric arrangement of *Rs*TspO. A: C2 symmetric homodimer model of *Rs*TspO in a ribbon representation fitted to the 10 Å EM map (EM Data Bank entry 1698). Transmembrane helices are labeled. The position of W38 is marked by an orange dot. The electron density is drawn at 1.65 σ level. B: Hydrophobicity analysis of TM1 of *Rs*TspO (top) and *m*TSPO (bottom). Helical wheel representation with nonpolar residues in yellow, polar residues in heather, glycines and alanines in gray, and prolines in green. The side of the helix that points to the interior of the helical bundle of *m*TSPO is marked by a dotted line. On top of the helical wheel, the respective primary sequence is shown. Only those residues exposed toward the membrane are colored. The overall hydrophobicity of TM1 of *Rs*TspO (top) and *m*TSPO is given inside each helical wheel. The hydrophobic moment is indicated by an arrow.

The best fit to the 10 Å EM map was obtained when the TM1 and TM2 helices were located at the dimer interface. In addition, the dimensions of the resulting *Rs*TspO dimer were in good agreement with those estimated from the EM map [Fig. 2(A)]. The relative orientation of the two subunits with respect to the *C*2 symmetry axis, which is parallel to the membrane normal, is mostly determined by the electron density corresponding to TM4 and TM5. Rotation of one subunit by ~34° around the *C*2 symmetry axis with respect to the best-fitting model shown in Figure 2(A) results in a worse fit of TM4 and TM5 to the experimental electron density [see Supporting Information Fig. S3(A)]. Moreover, placing helices TM2 and TM5 at the dimer interface resulted in a dimer that spans about 50 Å [see Supporting Information Fig. S3(B)], while EM estimates the maximum dimension to 40 Å. The experimental electron density of *Rs*TspO is less defined in the center of the lipid bilayer, in particular for the TM3 helix [Fig. 2(A)]. It was previously suggested that the low quality of the electron density map of *Rs*TspO is potentially due to interhelical motions,[19] in agreement with the dynamic nature of *m*TSPO in the absence of PK 11195.[12]

Discussion

Stabilization of the structure of *m*TSPO by PK 11195 was essential for its successful structure determination.[12] The structure of the *m*TSPO–PK 11195 complex is the first 3D high-resolution structure of a helical membrane protein in complex with a ligand solved by NMR spectroscopy. The perturbed interaction of bacterial TspO with synthetic ligands such as PK 11195 suggests that it might be even more difficult to determine the high-resolution structure of bacterial TspO. In addition, NMR spectroscopic studies of bacterial TspO such as *Rs*TspO are complicated by its propensity to assemble into homodimers.[19] On the other hand, it might be possible to stabilize the structure of the bacterial TspO by high-affinity natural ligands, such as tetrapyrroles, or synthetic ligands and thus enable high-resolution structural studies.

To obtain insight into the structural properties of bacterial TspO, we here combined the recently obtained knowledge about the 3D structure of mammalian TSPO[12] with bioinformatic analyses and an EM map of *Rs*TspO at 10 Å resolution.[19] In the structure of the *m*TSPO–PK 11195 complex, the extracellular side of *m*TSPO is stabilized by contacts between the TM1–TM2 loop and the TM5 helix. The connection between TM1 and TM2 folds onto the PK 11195 binding site, reducing the flexibility of the TSPO structure. In the derived 3D model of *Rs*TspO, however, the TM1–TM2 loop is shorter [Fig. 1(B) and Supporting Information Fig. S2].[25] In particular, the α-helix (E29 to A35) found in the TM1–TM2 loop of the *m*TSPO–PK 11195 complex, which is important for diagnostic ligand binding as supported by numerous mutagenesis experiments,[3,26] is not present. The absence of this α-helix could result in increased flexibility of the bacterial TM1–TM2 loop in comparison to mammalian TSPO. Moreover, the TM1 helix has the lowest interspecies similarities among the transmembrane domains of TspO/PBR proteins [Fig. 1(A) and Supporting Information Fig. S1]. For example, residues such as V26 of *m*TSPO, which directly contacts PK 11195, are not preserved in the *Rs*TspO sequence. At the same time, all TspO/PBR proteins bind tetrapyrrole intermediates of the heme biosynthetic pathway.[17] Bacterial *Rs*TspO can even be substituted with complete functionality by rat TSPO as a negative regulator for a number of photosynthetic genes.[27] The finding that both bacterial TspO and mammalian TSPO can bind tetrapyrrole substrates, but only mammalian TSPO has high affinity to PK 11195 suggests that the binding site for tetrapyrrole substrates differs at least partially from the binding site of synthetic ligands.[28]

Mutation of W38 in *Rs*TspO to cysteine results in formation of covalent dimers.[20] In the 3D model of *Rs*TspO, W38 is located above TM1/TM2 in the middle of the TM1–TM2 loop [Fig. 1(B)]. On the basis of the arrangement of the transmembrane helices, W38C-mediated disulfide bond formation is thus possible with two dimeric interfaces: TM1TM2:TM 2′TM1′ and TM2TM5:TM5′TM2′. However, only the dimer with the TM1TM2:TM2′TM1′ interface satisfies the dimensions of the EM density map [Fig. 2(A) and Supporting Information Fig. S3].[19] Support for the involvement of TM1 in the dimer interface also comes from the more polar character of TM1 in *Rs*TspO when compared to *m*TSPO [Fig. 2(B)]. In the monomeric *Rs*TspO model, several polar side chains of TM1 are located on the side that would point to the hydrophobic environment of the membrane [Fig. 2(B)]. Dimer formation mediated by these residues would therefore lower the energetics of membrane–TM interaction.[29–31] As additional support for the TM1TM2:TM2′TM1′ interface one might consider the residual electron density, which is present above the TM region close to the dimer interface and might be attributed to the disordered C-terminus of TM5 and the TM1–TM2 loop of *Rs*TspO [Fig. 2(A)]. A parallel orientation of the two subunits is in agreement with the EM map and the location of W38C (S41 in human/mouse ortholog).[20] Notably, residue C15, which is present only in the *Rs*TspO sequence and located in the middle of the TM1 helix [see Supporting Information Fig. S2], does not form a covalent disulfide bond between dimer subunits.[20] In the 3D model of *Rs*TspO, the C15 side chain is buried within the helical bundle [see Supporting Information Fig. S2].

According to the 3D structure of the mTSPO–PK 11195 complex, synthetic ligands of mammalian TSPO bind to a hydrophobic pocket formed by the bundle of five TM helices. In the dimeric model of *Rs*TspO shown in Figure 2(A), which is in agreement with the experimental electron density, some space is available within the 5-helix bundle of each subunit. This might point to two equivalent binding sites per dimer in bacterial TspO proteins. Similarly to the PK 11195 binding site of *m*TSPO, ligand binding to bacterial TspO proteins might involve TM4/TM4′ and TM5/TM5′, that is those transmembrane helices that were found to be the most stable elements of *m*TSPO after binding of PK 11195.[12] Two equivalent binding sites per bacterial TspO dimer are further supported by the finding that the A147T polymorphism, which occurs in TM5, affects both the binding of 2nd generation ligands to mammalian TSPO and interaction of porphyrin with bacterial TspO.[28,32] Alternatively, it has been suggested that the binding site for porphyrins might be located within the dimeric interface, as found in some multidrug transporters.[33,34] However, in the dimer model of *Rs*TspO [Fig. 2(A)], the dimer interface is rather flat and possibly tightly packed, questioning such a mechanism. Therefore, more studies are needed to investigate the stoichiometry of protein to ligand

binding in *Rs*TspO. In addition, dimeric or higher order oligomeric forms of *Rs*TspO might allow an allosteric interplay between ligand binding and protein oligomerization.

Mammalian TSPO can also oligomerize, but the underlying mechanism is unknown. Because the faces of the TM helices of *m*TSPO are predominantly hydrophobic, the mechanism of oligomerization likely differs from that of *Rs*TspO. One such mechanism could be *m*TSPO dimerization mediated by cholesterol. The cholesterol binding motif of *m*TSPO is on the membrane-oriented surface of TM5,[12] such that a cholesterol molecule could bind there, followed by dimerization with a second cholesterol molecule[35] and recruitment of a second *m*TSPO molecule. Indeed, cholesterol has been found in between the subunit structure of G-protein coupled receptors.[36] Bacterial membranes do not contain cholesterol, consistent with different aggregation modes of mammalian TSPOs and prokaryotic TspOs. In addition, reactive oxygen species can cause covalent oligomerization of *m*TSPO.[21]

In conclusion, the 3D model of TspO from *R. sphaeroides* developed on the basis of its 10 Å resolution EM map, the high-resolution 3D structure of *m*TSPO, and bioinformatic analysis provides molecular insights into the perturbed interaction of *Rs*TspO with high-affinity radioligands of mTSPO such as PK 11195. In addition, the developed arrangement of the *Rs*TspO dimer is in agreement with available data from EM and mutagenesis and suggests a mechanism for functional oligomerization of bacterial TspO proteins. Further validation of this model might include mutagenesis studies within the transmembrane helices TM1 and TM2, including covalent disulfide crosslinks, as well as titration studies with ligands in order to stabilize the protein fold for high-resolution structural studies.

Material and Methods

Multiple sequence alignment of 15 representatives of the TSPO protein family was performed using the T-COFFEE server[37] at http://www.ebi.ac.uk/Tools/msa/tcoffee/ (see Supporting Information Fig. S1). Figures were generated with Chimera version 1.8.1[22] using Multialign Viewer tools. Disordered fragments were predicted from the primary sequence using the PHYRE2 server (http://www.sbg.bio.ic.ac.uk/phyre2/).[38]

Comparative (homology) modeling of the monomeric *Rs*TspO subunit was done with the Chimera[22] interface to Modeller9v13[23] using full-atom mode including protons. The high resolution structure of *m*TSPO (PDB ID: 2MGY[12]) was used as a template together with the multiple sequence alignment of 15 TSPO family proteins (see Supporting Information Fig. S1). Because the NMR ensemble shows heterogeneity within the orientation of some side chains, all 20 structures from the ensemble were taken as templates for modeling. Each conformer was used to generate five models of *Rs*TspO resulting in 100 models in total. The highest-scored model was selected for further analysis. On the basis of the 3D structure of the *m*TSPO–PK 11195 complex[12] and the 3D model of *Rs*TspO, the physicochemical properties of the 18-residue-long TM1 helix of *m*TSPO and *Rs*TspO were analyzed using HeliQuest.[39]

The 10 Å resolution EM map of *Rs*TspO (EMDB id 1698[19]) was processed and analyzed using Chimera[22] version 1.8.1 at 1.65 σ level. The EM map was reduced to the asymmetric unit corresponding to the *Rs*TspO:*Rs*TspO dimer electron density and used for rigid body fitting of the 3D models of *Rs*TspO.

References

1. Anholt RR, Pedersen PL, De Souza EB, Snyder SH (1986) The peripheral-type benzodiazepine receptor. Localization to the mitochondrial outer membrane. J Biol Chem 261:576–583.
2. Fan J, Lindemann P, Feuilloley MG, Papadopoulos V (2012) Structural and functional evolution of the translocator protein (18 kDa). Curr Mol Med 12:369–386.
3. Li H, Papadopoulos V (1998) Peripheral-type benzodiazepine receptor function in cholesterol transport. Identification of a putative cholesterol recognition/interaction amino acid sequence and consensus pattern. Endocrinology 139:4991–4997.
4. Li H, Yao Z, Degenhardt B, Teper G, Papadopoulos V (2001) Cholesterol binding at the cholesterol recognition/interaction amino acid consensus (CRAC) of the peripheral-type benzodiazepine receptor and inhibition of steroidogenesis by an HIV TAT-CRAC peptide. Proc Natl Acad Sci USA 98:1267–1272.
5. Girard C, Liu S, Adams D, Lacroix C, Sineus M, Boucher C, Papadopoulos V, Rupprecht R, Schumacher M, Groyer G (2012) Axonal regeneration and neuroinflammation: roles for the translocator protein 18 kDa. J Neuroendocrinol 24:71–81.
6. Braestrup C, Albrechtsen R, Squires RF (1977) High densities of benzodiazepine receptors in human cortical areas. Nature 269:702–704.
7. Gavish M, Bachman I, Shoukrun R, Katz Y, Veenman L, Weisinger G, Weizman A (1999) Enigma of the peripheral benzodiazepine receptor. Pharmacol Rev 51: 629–650.
8. Papadopoulos V, Baraldi M, Guilarte TR, Knudsen TB, Lacapere JJ, Lindemann P, Norenberg MD, Nutt D, Weizman A, Zhang MR, Gavish M (2006) Translocator protein (18kDa): new nomenclature for the peripheral-type benzodiazepine receptor based on its structure and molecular function. Trends Pharmacol Sci 27:402–409.
9. McEnery MW, Snowman AM, Trifiletti RR, Snyder SH (1992) Isolation of the mitochondrial benzodiazepine receptor: association with the voltage-dependent anion channel and the adenine nucleotide carrier. Proc Natl Acad Sci USA 89:3170–3174.
10. Caballero B, Veenman L, Gavish M (2013) Role of mitochondrial translocator protein (18 kDa) on mitochondrial-related cell death processes. Recent Pat Endocr Metab Immune Drug Discov 7:86–101.

11. Gatliff J, Campanella M (2012) The 18 kDa translocator protein (TSPO): a new perspective in mitochondrial biology. Curr Mol Med 12:356–368.
12. Jaremko L, Jaremko M, Giller K, Becker S, Zweckstetter M (2014) Structure of the mitochondrial translocator protein in complex with a diagnostic ligand. Science 343:1363–1366.
13. Murail S, Robert JC, Coic YM, Neumann JM, Ostuni MA, Yao ZX, Papadopoulos V, Jamin N, Lacapere JJ (2008) Secondary and tertiary structures of the transmembrane domains of the translocator protein TSPO determined by NMR. Stabilization of the TSPO tertiary fold upon ligand binding. Biochim Biophys Acta 1778: 1375–1381.
14. Lacapere JJ, Delavoie F, Li H, Peranzi G, Maccario J, Papadopoulos V, Vidic B (2001) Structural and functional study of reconstituted peripheral benzodiazepine receptor. Biochem Biophys Res Commun 284:536–541.
15. Krueger KE, Papadopoulos V (1990) Peripheral-type benzodiazepine receptors mediate translocation of cholesterol from outer to inner mitochondrial membranes in adrenocortical cells. J Biol Chem 265:15015–15022.
16. Papadopoulos V, Mukhin AG, Costa E, Krueger KE (1990) The peripheral-type benzodiazepine receptor is functionally linked to Leydig cell steroidogenesis. J Biol Chem 265:3772–3779.
17. Taketani S, Kohno H, Okuda M, Furukawa T, Tokunaga R (1994) Induction of peripheral-type benzodiazepine receptors during differentiation of mouse erythroleukemia cells. A possible involvement of these receptors in heme biosynthesis. J Biol Chem 269:7527–7531.
18. Yeliseev AA, Krueger KE, Kaplan S (1997) A mammalian mitochondrial drug receptor functions as a bacterial "oxygen" sensor. Proc Natl Acad Sci USA 94:5101–5106.
19. Korkhov VM, Sachse C, Short JM, Tate CG (2010) Three-dimensional structure of TspO by electron cryomicroscopy of helical crystals. Structure 18:677–687.
20. Yeliseev AA, Kaplan S (2000) TspO of *Rhodobacter sphaeroides*. A structural and functional model for the mammalian peripheral benzodiazepine receptor. J Biol Chem 275:5657–5667.
21. Delavoie F, Li H, Hardwick M, Robert JC, Giatzakis C, Peranzi G, Yao ZX, Maccario J, Lacapere JJ, Papadopoulos V (2003) In vivo and in vitro peripheral-type benzodiazepine receptor polymerization: functional significance in drug ligand and cholesterol binding. Biochemistry 42:4506–4519.
22. Pettersen EF, Goddard TD, Huang CC, Couch GS, Greenblatt DM, Meng EC, Ferrin TE (2004) UCSF Chimera—a visualization system for exploratory research and analysis. J Comput Chem 25:1605–1612.
23. Eswar N, Webb B, Marti-Renom MA, Madhusudhan MS, Eramian D, Shen MY, Pieper U, Sali A (2006) Comparative protein structure modeling using Modeller. Curr Protoc Bioinformatics Chapter 5:Unit 5 6.
24. Wriggers W (2012) Conventions and workflows for using Situs. Acta Crystallogr D 68:344–351.
25. Teboul D, Beaufils S, Taveau JC, Iatmanen-Harbi S, Renault A, Venien-Bryan C, Vie V, Lacapere JJ (2012) Mouse TSPO in a lipid environment interacting with a functionalized monolayer. Biochim Biophys Acta 1818: 2791–2800.
26. Farges R, Joseph-Liauzun E, Shire D, Caput D, Le Fur G, Ferrara P (1994) Site-directed mutagenesis of the peripheral benzodiazepine receptor: identification of amino acids implicated in the binding site of Ro5–4864. Mol Pharmacol 46:1160–1167.
27. Zeng X, Kaplan S (2001) TspO as a modulator of the repressor/antirepressor (PpsR/AppA) regulatory system in *Rhodobacter sphaeroides* 2.4.1. J Bacteriol 183: 6355–6364.
28. Ginter C, Kiburu I, Boudker O (2013) Chemical catalysis by the translocator protein (18 kDa). Biochemistry 52:3609–3611.
29. Bayrhuber M, Meins T, Habeck M, Becker S, Giller K, Villinger S, Vonrhein C, Griesinger C, Zweckstetter M, Zeth K (2008) Structure of the human voltage-dependent anion channel. Proc Natl Acad Sci USA 105: 15370–15375.
30. Schredelseker J, Paz A, Lopez CJ, Altenbach C, Leung CS, Drexler MK, Chen JN, Hubbell WL, Abramson J (2014) High-resolution structure and double electron-electron resonance of the zebrafish voltage dependent anion channel 2 reveal an oligomeric population. J Biol Chem 289:12566–71257.
31. Naveed H, Jackups R Jr, Liang J (2009) Predicting weakly stable regions, oligomerization state, and protein–protein interfaces in transmembrane domains of outer membrane proteins. Proc Natl Acad Sci USA 106:12735–12740.
32. Owen DR, Yeo AJ, Gunn RN, Song K, Wadsworth G, Lewis A, Rhodes C, Pulford DJ, Bennacef I, Parker CA, StJean PL, Cardon LR, Mooser VE, Matthews PM, Rabiner EA, Rubio JP (2012) An 18-kDa translocator protein (TSPO) polymorphism explains differences in binding affinity of the PET radioligand PBR28. J Cerebral Blood Flow Metabol 32:1–5.
33. Dawson RJ, Locher KP (2006) Structure of a bacterial multidrug ABC transporter. Nature 443:180–185.
34. Ubarretxena-Belandia I, Baldwin JM, Schuldiner S, Tate CG (2003) Three-dimensional structure of the bacterial multidrug transporter EmrE shows it is an asymmetric homodimer. EMBO J 22:6175–6181.
35. Fantini J, Barrantes FJ (2013) How cholesterol interacts with membrane proteins: an exploration of cholesterol-binding sites including CRAC, CARC, and tilted domains. Front Physiol 4:31.
36. Cherezov V, Rosenbaum DM, Hanson MA, Rasmussen SG, Thian FS, Kobilka TS, Choi HJ, Kuhn P, Weis WI, Kobilka BK, Stevens RC (2007) High-resolution crystal structure of an engineered human beta2-adrenergic G protein-coupled receptor. Science 318:1258–1265.
37. Di Tommaso P, Moretti S, Xenarios I, Orobitg M, Montanyola A, Chang JM, Taly JF, Notredame C (2011) T-Coffee: a web server for the multiple sequence alignment of protein and RNA sequences using structural information and homology extension. Nucleic Acids Res 39:W13–17.
38. Kelley LA, Sternberg MJ (2009) Protein structure prediction on the Web: a case study using the Phyre server. Nat Protoc 4:363–371.
39. Gautier R, Douguet D, Antonny B, Drin G (2008) HELIQUEST: a web server to screen sequences with specific alpha-helical properties. Bioinformatics 24: 2101–2102.